Scientific Research Publishing

Journal of Modern Physics, 2022, 13, 932-948
https://www.scirp.org/journal/jmp
ISSN Online: 2153-120X
ISSN Print: 2153-1196

Warm Dark Matter and the Formation of First Galaxies

Bruce Hoeneisen

Universidad San Francisco de Quito, Quito, Ecuador
Email: bhoeneisen@usfq.edu.ec

How to cite this paper: Hoeneisen, B. (2022) Warm Dark Matter and the Formation of First Galaxies. *Journal of Modern Physics*, **13**, 932-948.
https://doi.org/10.4236/jmp.2022.136053

Received: May 2, 2022
Accepted: June 25, 2022
Published: June 28, 2022

Abstract

By numerical integration of hydro-dynamical equations, we study the formation of elliptical and spiral galaxies starting from primordial linear density-velocity-gravitational perturbations. Both dark matter and baryons are included. Warm dark matter perturbations acquire two low mass cut-offs: the free-streaming cut-off due to the power spectrum free-streaming cut-off factor $\tau^2(k)$, and the velocity dispersion cut-off. The Press-Schechter mass distribution does not include velocity dispersion, and should not be used below the velocity dispersion cut-off mass. From the formation of first galaxies and reionization, we estimate limits on the non-relativistic warm dark matter velocity dispersion at expansion parameter a: $v_{h\mathrm{rms}}(a) = v_{h\mathrm{rms}}(1)/a$, with $200\ \mathrm{m/s} \lesssim v_{h\mathrm{rms}}(1) \lesssim 395\ \mathrm{m/s}$.

Keywords

Warm Dark Matter, First Galaxies, First Stars, Population III Stars, Reionization

1. Introduction

Our aim is to try to understand dark matter. Our approach is data driven. Galaxies are our laboratory. We begin with a study of spiral galaxy rotation curves [1] [2]. Next, we study the formation of dark matter halos starting from primordial linear density-velocity-gravitational perturbations [3]. In the present work we extend the previous dynamical studies to include baryons. In particular, we study the formation of the first generation of galaxies and stars.

The root-mean-square velocity of non-relativistic dark matter particles depends on the expansion parameter a of the universe as follows:

$$v_{h\mathrm{rms}}(a) = \frac{v_{h\mathrm{rms}}(1)}{a}. \tag{1}$$

The cold dark matter ΛCDM cosmology assumes that dark matter particles have negligible velocity dispresion, *i.e.* $v_{h\mathrm{rms}}(1) \approx 0$. The warm dark matter ΛWDM scenario adds the single parameter $v_{h\mathrm{rms}}(1)$ to ΛCDM. The dark matter particle velocity dispersion results in a cut-off of the power spectrum of density fluctuations in the early universe due to free-streaming. The free-streaming cut-off wavenumber $k_{\mathrm{fs}}(t_{\mathrm{eq}})$, at the time of equal densities of radiation and matter, can be calculated from $v_{h\mathrm{rms}}(1)$ [4]. From the formation of first galaxies and reionization, we are able to set limits on $v_{h\mathrm{rms}}(1)$ and $k_{\mathrm{fs}}(t_{\mathrm{eq}})$.

In the following sections we discuss galaxy hydro-dynamical equations, their numerical solutions, the formation of first galaxies (that in ΛWDM depend on both the free-streaming power spectrum cut-off factor $\tau^2(k)$, and on the dark matter velocity dispersion), comment on the formation of first galaxies and stars in nodes, filaments and sheets, and estimate limits on the warm dark matter velocity dispersion based on the formation of first galaxies and reionization. We conclude with a brief comparison with previous measurements, and mention discrepancies with dark matter limits in the literature.

We use the standard notation in cosmology, and the cosmological parameters as in [5]. Throughout, the subscript *h* stands for the dark matter halo, and *b* stands for baryons.

2. Equations for Warm Dark Matter and Baryons

The formation of the galactic halo can be illustrated by integrating numerically Newton's equation

$$\nabla \cdot \boldsymbol{g} = -4\pi G\left(\rho_h + \rho_b\right), \tag{2}$$

the continuity equations

$$\frac{\partial \rho_h}{\partial t} = -\nabla \cdot \left(\boldsymbol{v}_h \rho_h\right), \tag{3}$$

$$\frac{\partial \rho_b}{\partial t} = -\nabla \cdot \left(\boldsymbol{v}_b \rho_b\right), \tag{4}$$

and Euler's equations

$$\frac{\mathrm{d}\boldsymbol{v}_h}{\mathrm{d}t} = \frac{\partial \boldsymbol{v}_h}{\partial t} + \left(\boldsymbol{v}_h \cdot \nabla\right)\boldsymbol{v}_h = \left(1-\kappa_h(t)\right)\boldsymbol{g} - \frac{1}{\rho_h}\nabla\left(\left\langle v_{rh}^2\right\rangle \rho_h\right). \tag{5}$$

$$\frac{\mathrm{d}\boldsymbol{v}_b}{\mathrm{d}t} = \frac{\partial \boldsymbol{v}_b}{\partial t} + \left(\boldsymbol{v}_b \cdot \nabla\right)\boldsymbol{v}_b = \left(1-\kappa_b(t)\right)\boldsymbol{g} - \frac{1}{\rho_b}\nabla\left(\left\langle v_{rb}^2\right\rangle \rho_b\right). \tag{6}$$

$\boldsymbol{g}(\boldsymbol{x})$ is the gravitation field, $\boldsymbol{x}$ is the proper coordinate vector, $\rho_h(\boldsymbol{x})$ and $\rho_b(\boldsymbol{x})$ are the mass densities, $\boldsymbol{v}_h(\boldsymbol{x})$ and $\boldsymbol{v}_b(\boldsymbol{x})$ are the velocities, and $\sqrt{\left\langle v_{rh}^2\right\rangle}$ and $\sqrt{\left\langle v_{rb}^2\right\rangle}$ are the radial (1-dimensional) velocity dispersions, of dark matter and baryons (hydrogen and helium), respectively. Equations (5) and (6) express the conservation of momentum. We use proper, not comoving, spatial coordinates. The functions $\kappa_h(t)$ and $\kappa_b(t)$ are included to describe spiral galaxy rotation [1] [2] [6]. We will discuss these functions below. For warm dark

matter we supplement the preceding equations with the condition of adiabatic expansion in the core of the galaxy:

$$\sqrt{\left\langle v_{rh}^2 \right\rangle} = \frac{v_{h\mathrm{rms}}(1)}{\sqrt{3}} \left(\frac{\rho_h(r_{\min}, t)}{\Omega_c \rho_{\mathrm{crit}}} \right)^{1/3}. \tag{7}$$

This condition is studied in [3]. Similarly, while the hydrogen and helium gas remains adiabatic, *i.e.* until excitations, radiation and shocks become significant, we require

$$\sqrt{\left\langle v_{rb}^2 \right\rangle} = \frac{v_{b\mathrm{rms}}(1)}{\sqrt{3}} \left(\frac{\rho_b(r_{\min}, t)}{\Omega_b \rho_{\mathrm{crit}}} \right)^{1/3} \tag{8}$$

in the core of the galaxy. For baryons we take $v_{b\mathrm{rms}}(1) = 21$ m/s, corresponding to hydrogen decoupling from photons at $z \approx 150$ [7]. We have made several data driven approximations [1] [3]: $\left\langle v_{rh}^2 \right\rangle$, $\left\langle v_{rb}^2 \right\rangle$, $\kappa_h(t)$, and $\kappa_b(t)$ are taken to be independent of *r*, and hence, the adiabatic constraints (7) and (8) are applied, at each time step in the numerical integration, only at $r_{\min}$.

Static solutions of Equations (2), (5) and (6) are studied in [1] and [3]. The static solutions depend on the variables $\left\langle v_{rh}'^2 \right\rangle \equiv \left\langle v_{rh}^2 \right\rangle / (1-\kappa_h)$, and $\left\langle v_{rb}'^2 \right\rangle \equiv \left\langle v_{rb}^2 \right\rangle / (1-\kappa_b)$. For elliptical galaxies we may take $\kappa_h \approx 0$ and $\kappa_b \approx 0$. For spiral galaxies we estimate $\kappa_h \approx 0$ and $\kappa_b \approx 0.98$ [1]. We solve the static equations by numerical integration, starting from the radius $r_{\min}$ of the first measured rotation velocity, up to $r_{\max}$ of the last one. To begin these integrations we need four boundary conditions: the radial velocity dispersions $\sqrt{\left\langle v_{rh}^2 \right\rangle}$ and $\sqrt{\left\langle v_{rb}^2 \right\rangle}$, and the densities $\rho_h(r_{\min})$ and $\rho_b(r_{\min})$, of dark matter and baryons, respectively. We vary these four parameters to minimize a χ^2 between the calculated and measured rotation curves. Good fits to the data are obtained assuming $\sqrt{\left\langle v_{rh}^2 \right\rangle}$ and $\sqrt{\left\langle v_{rb}^2 \right\rangle}$ are independent of *r*. We predict that the adiabatic invariant $\sqrt{\left\langle v_{rh}^2 \right\rangle} / \rho_h(r \to 0)^{1/3}$ is of cosmological origin, and hence has the same value for all relaxed spiral galaxies [3]. From measurements of approximately 60 spiral galaxies, we obtain the adiabatic invariant

$$v_{h\mathrm{rms}}(1) \equiv \sqrt{3} \sqrt{\left\langle v_{rh}^2 \right\rangle} \left(\frac{\Omega_c \rho_{\mathrm{crit}}}{\rho_h(r \to 0)} \right)^{1/3} = 0.79 \pm 0.33\,(\mathrm{tot})\ \mathrm{km/s}, \tag{9}$$

at 68% confidence [8]. The conclusion is that dark matter is (arguably) warm. The velocity dispersion (9) corresponds to a warm dark matter power spectrum cut-off wavenumber, due to free-streaming, $k_{\mathrm{fs}}(t_{\mathrm{eq}}) = 1.03^{+0.74}_{-0.30}\ \mathrm{Mpc}^{-1}$, at equality of the densities of radiation and matter [4] [8]. In summary, relaxed spiral galaxy density runs $\rho_h(r)$ and $\rho_b(r)$ are described by only three independent parameters. Note that $v_{b\mathrm{rms}}(1) \ll v_{h\mathrm{rms}}(1)$, so baryons act like cold dark matter.

The static equations have been extended to degenerate fermion or boson dark matter [1] [6]. The onset of degeneracy brings disagreement with spiral galaxy rotation curves, so lower limits are set on the dark matter particle mass m_h [1] [6].

Dynamic, spherically symmetric, solutions to Equations (2) to (8) are studied in [3] for the case of no baryons. In the cold dark matter scenario the dark matter particles fall to the origin, overshoot, splash-back, overshoot again, and relaxation phenomena are invoked to "virialize the galaxy" [9]. In the warm dark matter scenario, the dark matter halo may form adiabatically, due to the feedback from (7) that halts the halo collapse, reaching a relaxed density run $\rho_h(r)$ with the following asymptotes: the core density ρ_c extends out to the core radius [3]

$$r_c \equiv \left[\frac{\langle v'^2_{rh}\rangle}{2\pi G\rho_c}\right]^{1/2}, \tag{10}$$

and thereafter $\rho_h(r)$ and $M_h(<r)$ approach

$$\rho_h(r) = \frac{\langle v'^2_{rh}\rangle}{2\pi G r^2}, \quad M_h(<r) = \frac{2\langle v'^2_{rh}\rangle}{G} r. \tag{11}$$

The only independent parameter is $\sqrt{\langle v'^2_{rh}\rangle}$, since ρ_c can then be obtained from the adiabatic invariant (7). $\sqrt{\langle v'^2_{rh}\rangle}$ is obtained by numerical integration starting from the initial linear density-velocity-gravitational perturbation. The radius of the warm dark matter halo keeps growing with constant speed $\sqrt{3\langle v'^2_{rh}\rangle}$, so the halo mass keeps increasing linearly with time, and no well defined static "virialized" halo mass can be defined. Note that the core is (arguably) evidence for warm dark matter. In the present work we extend these studies to include baryons.

3. Simulations

As an example, let us consider the evolution of an initial spherically symmetric Gaussian perturbation. The initial densities, at expansion parameter a_i, are $\rho_{hi}(r) = \rho_i(r)\Omega_c/(\Omega_c+\Omega_b)$, and $\rho_{bi}(r) = \rho_i(r)\Omega_b/(\Omega_c+\Omega_b)$, with

$$\rho_i(r) = \bar{\rho}_i\left[1+\delta\exp\left(-\frac{r^2}{r_i^2}\right)\right]. \tag{12}$$

The initial velocities are $v_{rhi}(r) = v_{rbi}(r) = H(a_i)r\left[1-(\bar{\rho}_{<r}-\rho_0)/(3\rho_0)\right]$, corresponding to a growing mode. The average $\bar{\rho}_{<r}$ is taken with weight r^2. The initial parameters are $z_i = 135$, $\bar{\rho}_i = 0.1 M_\odot\ \mathrm{pc}^{-3}$, $\delta = 0.3$, and $r_i = 4$ kpc. The linear dark matter and baryon masses are $M_h = 2.3\times10^{10} M_\odot$ and $M_b = 4.2\times10^9 M_\odot$, respectively. Note that we have assumed that baryons track dark matter while perturbations are linear for the masses of interest (much greater than M_{JbW} to be defined below). We assume cold dark matter. We assume no angular momentum, so set $\kappa_h(t) = \kappa_b(t) = 0$. Numerical integration of Equations (2) to (8) with these initial conditions are shown in **Figure 1**. We note that $\rho_h(r,t)$ remains equal to $\Omega_c\rho_b(r,t)/\Omega_b$, *i.e.* baryons act as cold dark matter. Our code crashes when $\rho_h(r)$ and $\rho_b(r)$ diverge at $r\to 0$. The equations are no longer valid beyond the collapse of dark matter or baryons

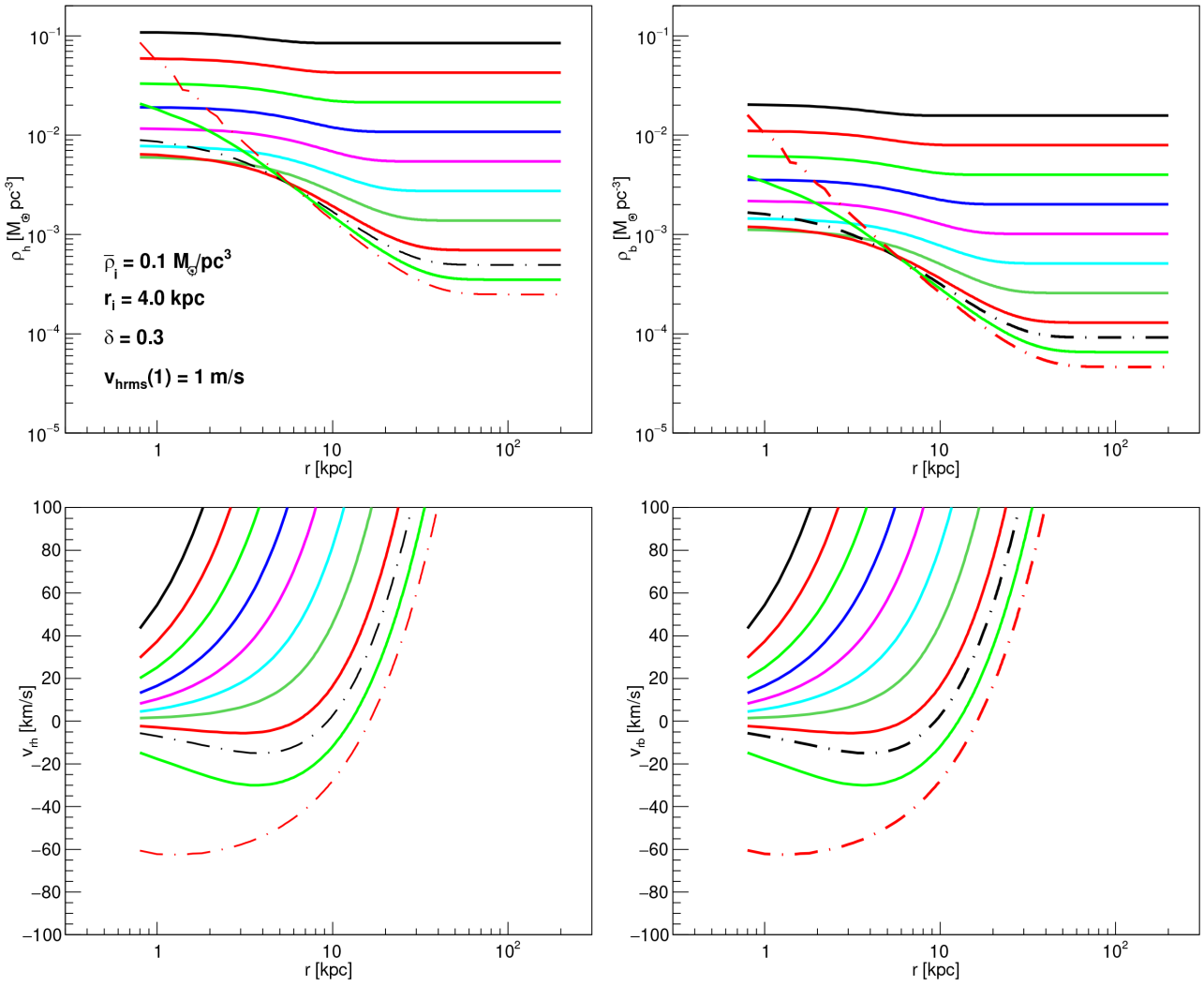

Figure 1. The formation of a cold dark matter plus baryon galaxy with zero angular momentum is shown. $\rho_h(r)$, $\rho_b(r)$, $v_{rh}(r)$, and $v_{rb}(r)$ are presented at time-steps that increase by factors 1.4086 (or $\sqrt{1.4086}$ for the dot-dashed lines). The initial perturbation is Gaussian, with parameters listed in the figure. The linear masses are $M_h = 2.3\times10^{10} M_\odot$ and $M_b = 4.2\times10^{9} M_\odot$.

at the origin.

For comparison, in **Figure 2** we present the formation of a similar galaxy, but with warm dark matter with $v_{hrms}(1) = 790$ m/s, corresponding to $k_{fs} = 1\ \text{Mpc}^{-1}$. The result is qualitatively different. The proportionality between $\rho_h(r,t)$ and $\rho_b(r,t)$ is lost. We note that the formation of the warm dark matter halo is delayed with respect to the corresponding cold dark matter case of **Figure 1**. The warm dark matter halo approaches a relaxed core, while baryons approach a "mini" core (not resolved by this simulation), and baryon radiation becomes important.

The collapse of baryons is halted if baryons have an angular momentum. To investigate this phenomenon, we set $\kappa_h(t) = 0$, and begin the numerical integration with $\kappa_b(t_i) \approx 0$, e.g. $\kappa_b(t_i) = 0.0001$, and gradually increase $\kappa_b(t)$ to 1 so as to conserve the baryon angular momentum. Let v_{rot} be the velocity of a

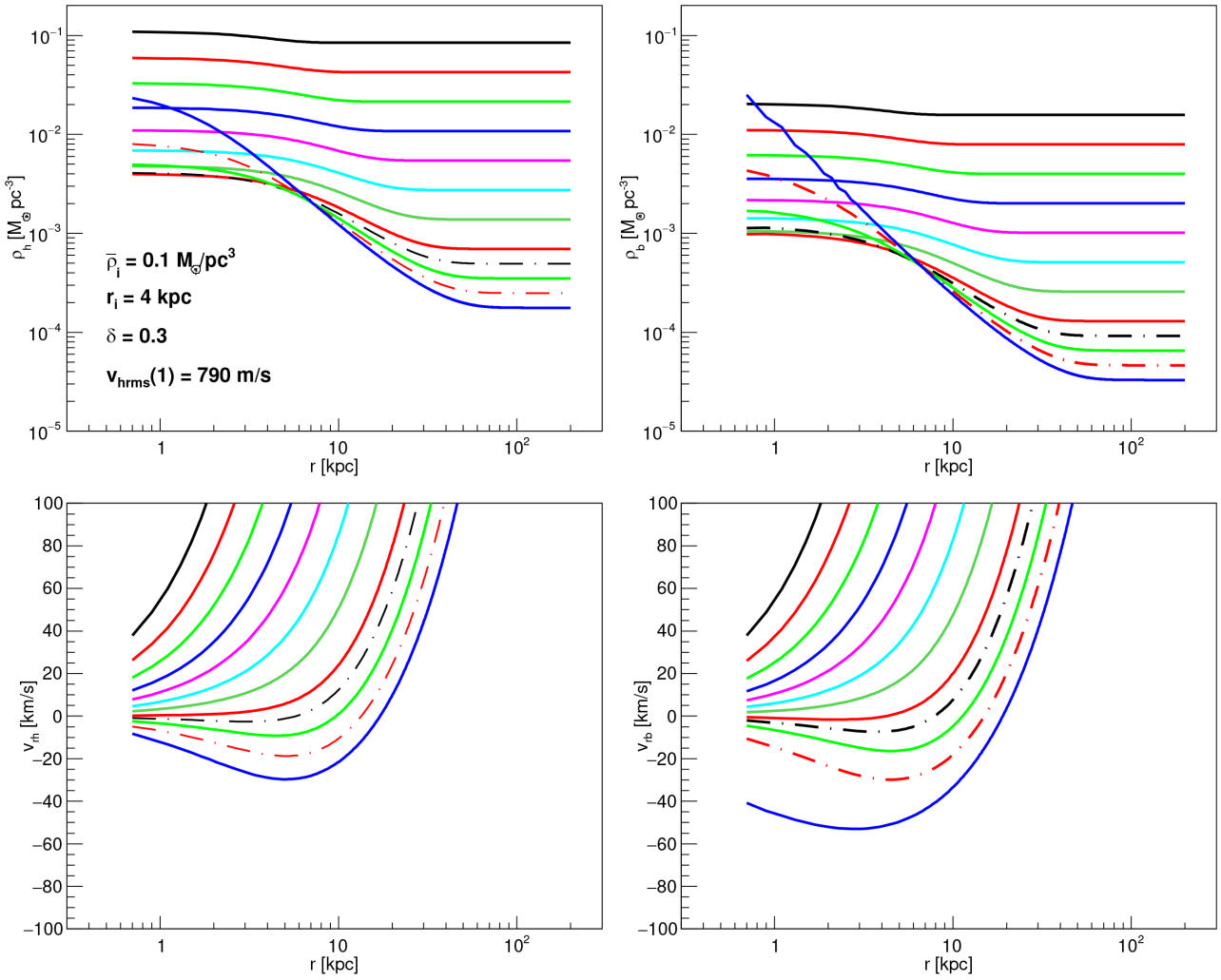

Figure 2. The formation of a warm dark matter plus baryon galaxy with zero angular momentum is shown. $\rho_h(r)$, $\rho_b(r)$, $v_{rh}(r)$, and $v_{rb}(r)$ are presented at time-steps that increase by factors 1.4086 (or $\sqrt{1.4086}$ for the dot-dashed lines). The initial perturbation is Gaussian, with parameters listed in the figure. Dark matter is warm with $v_{hrms}(1) = 790$ m/s, corresponding to $k_{fs} = 1\ \text{Mpc}^{-1}$. The linear masses are $M_h = 2.3\times10^{10} M_\odot$ and $M_b = 4.2\times10^{9} M_\odot$.

test particle in a circular orbit of radius r. Then $g = -v_{\text{rot}}^2/r$. Let $v_{b\text{rot}}$ be the rotation velocity of baryons at radius r. Then $\kappa_b(t) = v_{b\text{rot}}^2/v_{\text{rot}}^2$. As a working approximation we take $\kappa_b(t)$ independent of r. The baryon angular momentum is

$$L_b = \int r v_{b\text{rot}} \rho_b(r)\,\mathrm{d}V. \tag{13}$$

The rotating baryons approach a disk, so we approximate

$$L_b \propto \int_0^\infty r^{5/2}\sqrt{-\kappa_b(t)\,g(r)}\,\rho_b(r)\,\mathrm{d}r. \tag{14}$$

This expression becomes well defined, *i.e.* finite, if $\rho_b(r)$ decreases faster than r^{-3}. This becomes the case due to baryon energy loss by radiation. An example as in Figure 2, but with baryons with an initial angular momentum, is presented in Figure 3. We note that both warm dark matter and baryons reach relaxed

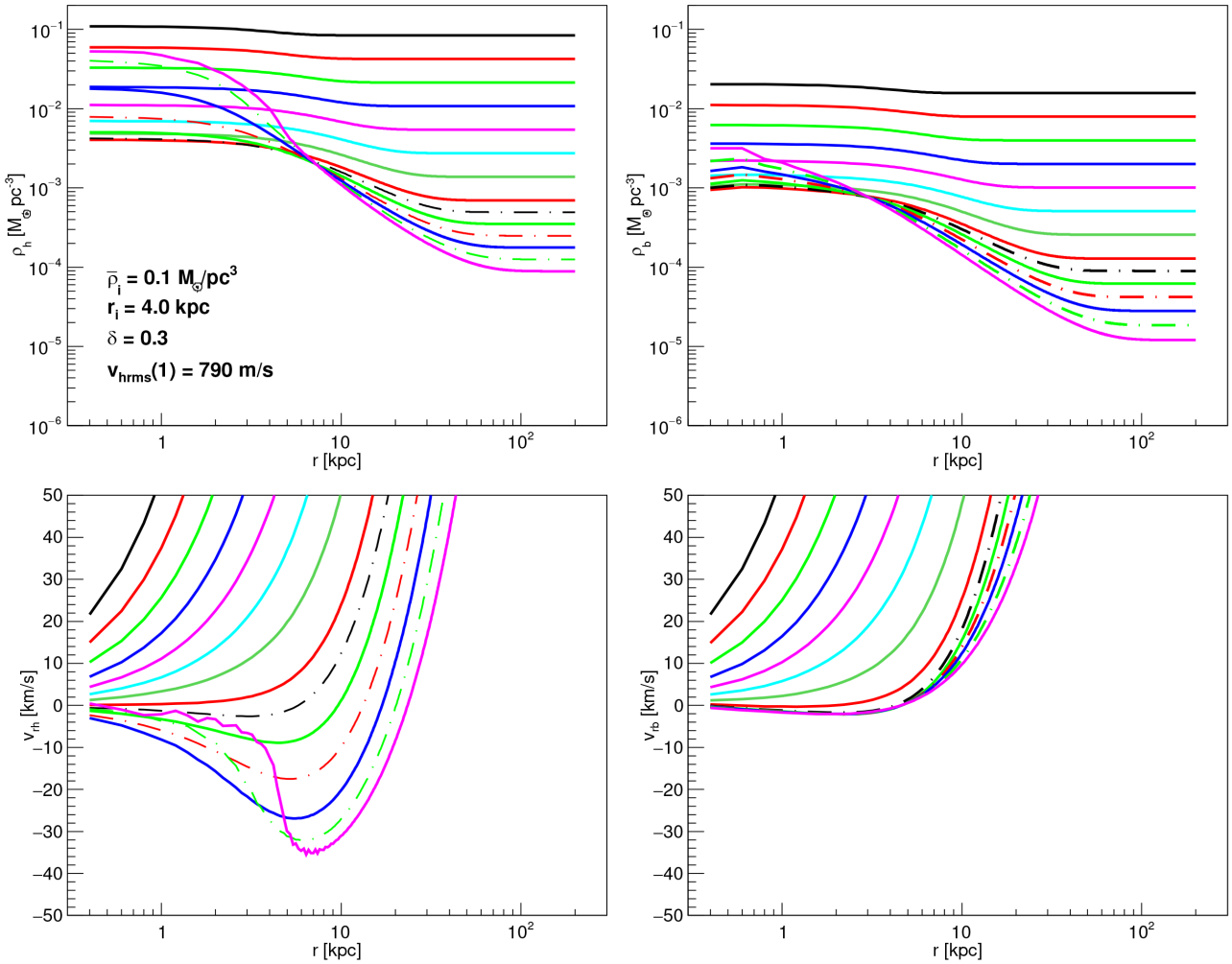

Figure 3. Shown is the formation of a warm dark matter plus baryon galaxy, as in **Figure 2**, but with baryon angular momentum. $\rho_h(r)$, $\rho_b(r)$, $v_{rh}(r)$, and $v_{rb}(r)$ are presented at time-steps that increase by factors 1.4086 (or $\sqrt{1.4086}$ for the dot-dashed lines). The initial perturbation is Gaussian, with parameters listed in the figure. Dark matter is warm with $v_{hrms}(1) = 790$ m/s, corresponding to $k_{fs} = 1\,\mathrm{Mpc}^{-1}$. $\kappa_h(t) = 0$. $\kappa_b(t)$ is increased from 10^{-4} to 1 keeping constant baryon angular momentum. The linear masses are $M_h = 2.3\times10^{10} M_\odot$ and $M_b = 4.2\times10^{9} M_\odot$. Note that both warm dark matter and baryons acquire cores. The baryon core is due to the baryon angular momentum conservation. Note the effect of the warm dark matter adiabatic feedback on $v_{rh}(r)$ at the final times shown (studied in [3]). A steady state is reached for both warm dark matter and baryons.

cores. In this way we are able to follow the formation of both relaxed elliptical and spiral galaxies starting from initial linear perturbations.

Keeping the spherical symmetry, we are also able to study the collapse of baryons in warm dark matter spherical sheets, see **Figure 4**. Note how baryons shock at collapse.

In **Figure 5** we illustrate that no self-gravitating structure is formed if the linear mass M of the perturbation is below a threshold.

4. First Galaxies

Let us define "first galaxy". The definition needs to be of a probabilistic nature,

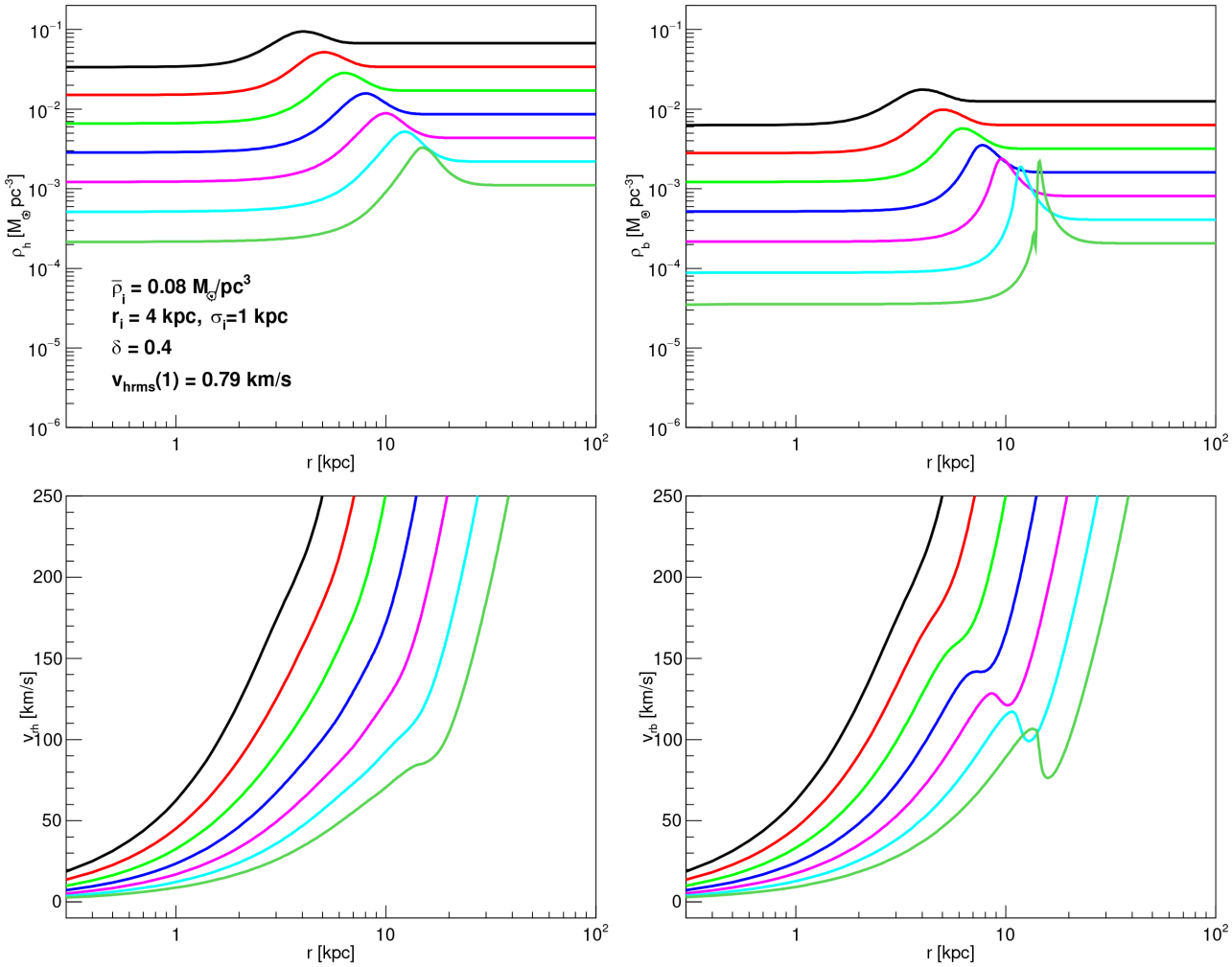

Figure 4. We illustrate the collapse of baryons in a spherical sheet of dark matter. $\rho_h(r)$, $\rho_b(r)$, $v_{rh}(r)$, and $v_{rb}(r)$ are presented at time-steps that increase by factors 1.4086. Dark matter is warm with $v_{hrms}(1) = 790$ m/s, corresponding to $k_{fs} = 1\,\mathrm{Mpc}^{-1}$.

since, with a sufficiently large volume, it is possible to find a galaxy before the "first galaxy". To this end, let us recall the variance of relative warm dark matter density perturbations $\delta(\boldsymbol{x}) \equiv (\rho(\boldsymbol{x}) - \bar{\rho})/\bar{\rho}$ on the linear mass scale M, at redshift z: [7]

$$\sigma^2(M, z, k_{fs}) = \frac{f^2}{(2\pi)^3 (1+z)^2} \int_0^\infty 4\pi k^2 \mathrm{d}k P(k) \tau^2(k) W^2(k). \quad (15)$$

f is a correction due to the accelerated expansion of the universe: $f = 1, 1.252, 1.269$ for redshift $z = 0, 2, 11$ respectively. k is the comoving wavenumber. $W(k)$ is a window function that defines the total (dark matter plus baryon) linear mass M. $P(k)$ is the ΛCDM linear relative density power spectrum at $z = 0$ (we use the analytic expression in [7]). $\tau^2(k)$ is a cut-off factor due to warm dark matter free-streaming. We take $\tau^2(k) \approx \exp(-k^2/k_{fs}^2)$ [4], where k_{fs} is the warm dark matter free-streaming comoving cut-off wavenumber. Note our definition of k_{fs}: $\tau^2(k_{fs}) \equiv e^{-1}$. $P'(k) \equiv f^2 P(k) \tau^2(k) / (1+z)^2$ is the

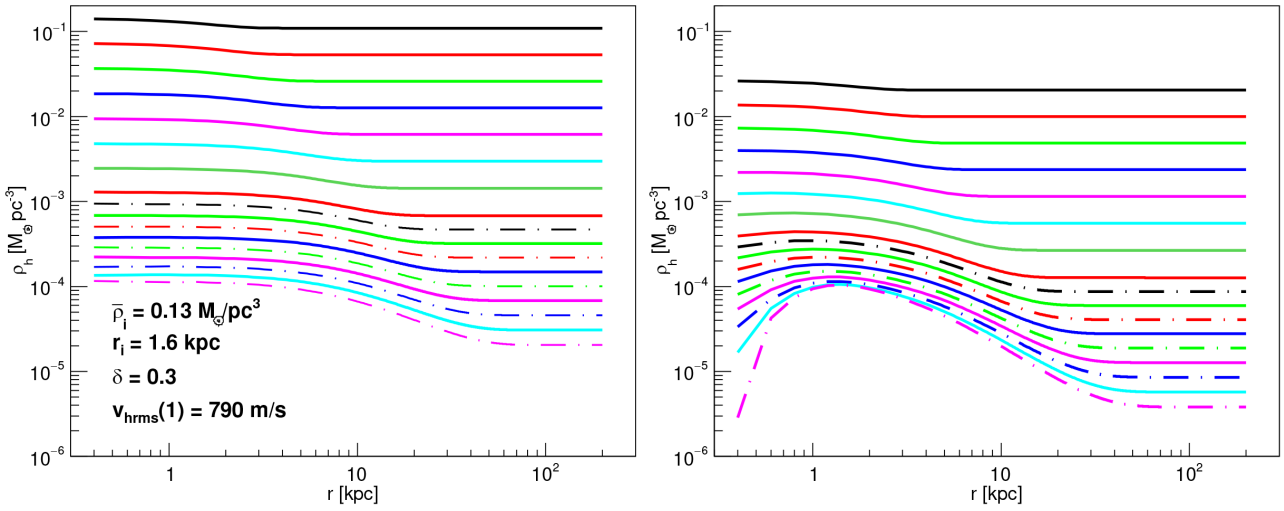

Figure 5. Shown is the evolution of an initial Gaussian perturbation, with the parameters listed in the figure, and with zero angular momentum. $\rho_h(r)$, $\rho_b(r)$, $v_{rh}(r)$, and $v_{rb}(r)$ are presented at time-steps that increase by factors 1.4086 (or $\sqrt{1.4086}$ for the dot-dashed lines). Dark matter is warm with $v_{hrms}(1) = 790$ m/s, corresponding to $k_{fs} = 1\,\text{Mpc}^{-1}$. The linear masses are $M_h = 1.9\times10^9 M_\odot$ and $M_b = 3.5\times10^8 M_\odot$. No timely self-gravitating structure is formed for masses less than $M = M_h + M_b$. The downturn of $\rho_b(r\to 0)$ at late times is due to accumulating numerical errors near the core that is not simulated.

proper power spectrum at redshift *z*. For each k_{fs} we adjust the amplitude of $P(k)$ so that $\sigma_8 = 0.811$ [5], calculated with a top-hat window function of radius $8/h$ Mpc. For all other calculations we use the well behaved Gaussian window function (see [8] for details):

$$W(k) = \exp\left(-\frac{k^2}{2k_0^2}\right), \quad M = \frac{4}{3}\pi\left(\frac{1.555}{k_0}\right)^3 \bar{\rho}_m. \tag{16}$$

In the ΛCDM scenario, when $\delta(\boldsymbol{x})$ reaches 1.686 in the linear approximation, the true value of $\delta(\boldsymbol{x})$ diverges (for a spherically symmetric perturbation), and a galaxy forms. This is also true for the ΛWDM scenario for sufficiently large *M* so that velocity dispersion is negligible, *i.e.* above the "dots" in **Figures 6-8** below. At $z = 8$, galaxies with $\log_{10}(M_*/M_\odot) = 9.05$ (9.55) (see distributions in [6]) correspond to fluctuations $1.686/\sigma(M_*(\Omega_c+\Omega_b)/\Omega_b, z, \infty) = 3.0$ (3.4) standard deviations in the ΛCDM scenario if recently formed. At $z = 6$, galaxies with $\log_{10}(M_*/M_\odot) = 9.05$ (10.7) correspond to fluctuations of 2.3 (3.7) standard deviations. Note that the redshift at half reionization is $z = 7.7\pm0.7$ [5]. Guided by these data, we *define* "first galaxy" (or "first star", as the case may be) as a galaxy that forms from a 4 standard deviation fluctuation.

In the present article we consider the ΛCDM scenario, and several ΛWDM scenarios: ΛWDM_1 with $v_{hrms}(1) = 0.79$ km/s, and the corresponding $k_{fs}(t_{eq}) = 1.0\ \text{Mpc}^{-1}$; ΛWDM_2 with $v_{hrms}(1) = 0.395$ km/s and $k_{fs}(t_{eq}) = 2.0\ \text{Mpc}^{-1}$; and ΛWDM_4 with $v_{hrms}(1) = 0.2$ km/s and $k_{fs}(t_{eq}) = 4.0\ \text{Mpc}^{-1}$.

Let us understand **Figure 6**. The horizontal axis is the redshift *z*. Time $t \propto (1+z)^{-3/2}$ advances towards the left. The vertical axis is the linear baryon

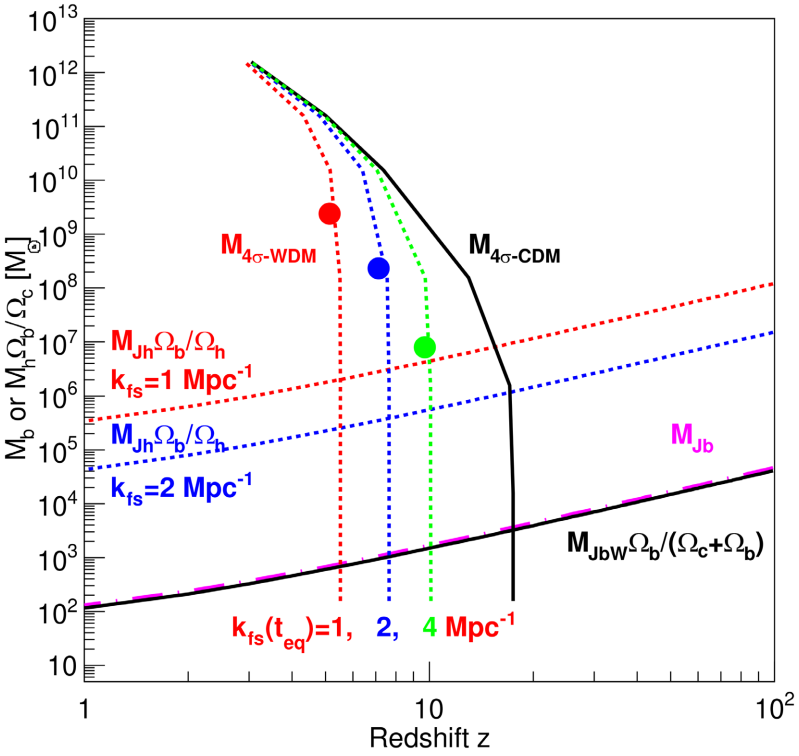

Figure 6. The following linear masses are presented as a function of redshift z: the baryon only Jeans mass M_{Jb}, the warm dark matter only Jeans masses M_{Jh} (times Ω_b/Ω_c) for the ΛWDM_1 and ΛWDM_2 scenarios, and the baryon mass for cold dark matter halos with a full complement of baryons $M_{JbW}\Omega_b/(\Omega_c+\Omega_b)$, see text. Also presented are linear masses for the ΛWDM_1, ΛWDM_2, ΛWDM_4, and ΛCDM scenarios for which 4σ spherically symmetric fluctuations collapse. These lines are only valid above the dots, see text. Non-linear regeneration of small scale structure is not included.

mass M_b (or the linear dark matter mass M_h times Ω_b/Ω_c for the dark matter-only lines with short-dash style). Linear masses are well defined, since a linear, *i.e.* a relatively small, density perturbation has dimensions that scale as the expansion parameter a, and a density that scales as a^{-3}, so the linear mass of a fluctuation is independent of a. The nearly vertical lines are defined by $\sigma\left(M_b\left(\Omega_c+\Omega_b\right)/\Omega_b, z, k_{\text{fs}}\right)=1.686/4$ with $k_{\text{fs}}=1,2,4,\infty$ Mpc^{-1} for the ΛWDM_1, ΛWDM_2, ΛWDM_4, and ΛCDM scenarios, respectively.

For completeness, we also present in **Figure 6** several proper Jeans masses (with nearly horizontal lines). The warm dark matter Jeans mass M_{Jh}, for the case of no baryons, derived from the linear approximations of (2), (3) and (5), is

$$M_{Jh}=\frac{4}{3}\pi\left(\frac{1.555}{k_{Jh}}\right)^3\bar{\rho}_h, \tag{17}$$

$$k_{Jh}\equiv\frac{2\pi}{\lambda_{Jh}},\quad \lambda_{Jh}=\sqrt{\frac{\left\langle v_{rh}'^2\right\rangle\pi}{G\bar{\rho}_h}}, \tag{18}$$

with all variables evaluated at redshift z. The short-dash lines correspond to the ΛWDM_1 and ΛWDM_2 scenarios. For the ΛCDM scenario, $M_{Jh}\approx 0$. Linear

dark matter perturbations with mass greater than M_{Jh} grow due to self-gravitation, while perturbations with mass less than M_{Jh} are attenuated.

The curve marked M_{Jb} is the Jeans mass of baryons, for the case of no dark matter. It is calculated as above, but with the proper Jeans length

$$\lambda_{Jb} = \sqrt{\frac{v_s^2 \pi}{G\bar{\rho}_b}}, \quad v_s = \sqrt{\frac{5kT_b}{3\mu m_p}}. \tag{19}$$

v_s is the sound velocity in a gas of hydrogen and helium with mean molecular weight $\mu = 1.22$ [7]. The baryon temperature $T_b(a)$ is calculated assuming baryons decouple from photons at $z \approx 150$ [7], and thereafter $T_b(a) \propto a^{-2}$. Thus, we take $T_b(1) = 2.7/151\,\mathrm{K}$. Assuming no dark matter, linear baryon perturbations with mass greater than M_{Jb} grow due to self-gravitation, while perturbations with mass less than M_{Jb} propagate as sound waves.

The curve marked M_{JbW} is a sort of Jeans mass for the ΛCDM scenario. In this scenario, linear perturbations of arbitrarily small dark matter mass can collapse, but with a reduced baryon fraction due to baryon pressure, unless the linear dark matter plus baryon perturbation mass is greater than [7]

$$M_{JbW} = \left(\frac{\pi}{G}\right)^{3/2} \frac{v_s^3}{\bar{\rho}_m^{1/2}}. \tag{20}$$

The line corresponding to k_{fs} in **Figure 6** is accurate above the dot, *i.e.* above the *velocity dispersion* cut-off. Below the dot, warm dark matter velocity dispersion becomes important, and lowers the redshift of baryon collapse, and finally prevents the formation of self-gravitating structures, see **Figure 5**. To obtain the "dot" we proceed as follows. We choose a δ for the simulations, e.g. $\delta = 0.3$. We choose a mass M_b. Then, from **Figure 6** we read off the redshift z_C at which the galaxy forms in the ΛCDM scenario. Then, from $\delta/\left((1+z_C)a_i\right) = 1.686$ we obtain the initial expansion parameter a_i, the initial mean matter density $\bar{\rho}_i$, and the initial radius r_i, for the simulation. We then run the simulation with $v_{h\mathrm{rms}}(1) = 0$ for ΛCDM, and the corresponding $v_{h\mathrm{rms}}(1)$ for the ΛWDM scenario, and obtain the difference in redshift Δz of galaxy formation in these two simulations. We place the "dot" at the mass M_b that obtains $\Delta z = 1$. Above the dot, the effect of the velocity dispersion can be neglected. Below the dot, velocity dispersion lowers the redshift of galaxy formation, if the galaxy forms at all (see **Figure 5** above), and the curve in **Figure 6** becomes invalid. The initial expansion parameter a_i of the simulation is not critical.

Warm dark matter perturbations acquire two low mass cut-offs: the *free-streaming* cut-off due to the power spectrum free-streaming cut-off factor $\tau^2(k)$, and the *velocity dispersion* cut-off, *i.e.* the dots in **Figures 6-8**. The Press-Schechter linear galaxy mass distribution [10] includes the *free-streaming* cut-off, but does not include the *velocity dispersion* cut-off. Care should be taken not to apply the Press-Schechter relation to perturbations below the *velocity dispersion* cut-off mass.

We are now in a position to understand **Figure 6**. Considering only spherically symmetric perturbations, and neglecting non-linear regeneration of small scale structure, we obtain the following results. For the ΛWDM_1, ΛWDM_2 and ΛWDM_4 scenarios, "first galaxies" and stars form approximately at the red, blue and green dots, for $k_{fs}\left(t_{eq}\right)=1\ \text{Mpc}^{-1}, 2\ \text{Mpc}^{-1}$ and 4 Mpc^{-1}, at $z\approx 5.5, 7.6$ and 10.1, and $M_b\approx 3\times 10^9 M_\odot, 3\times 10^8 M_\odot$ and $1\times 10^7 M_\odot$, respectively. For the ΛCDM scenario, "first halos" (with 4σ fluctuations) with a full complement of baryons, *i.e.* first galaxies and stars, form approximately when the two black lines meet at $z\approx 18$ and $M_b\approx 5\times 10^3 M_\odot$. If we only consider spherically symmetric perturbations, and neglect non-linear regeneration of small scale structure, we conclude that the warmest dark matter consistent with reionization has $v_{hrms}(1)\approx 270$ m/s, $k_{fs}\approx 3\ \text{Mpc}^{-1}$, and first galaxies have masses of order $10^8 M_\odot$ (these may break up).

These results are approximate because we have only considered spherically symmetric perturbations, and have not included non-linear regeneration of small scale structure. An ellipsoidal perturbation collapses first along its shortest axis (obtaining a Zeldovich pancake or sheet), then along the intermediate axis (obtaining a filament), and finally along the longest axis (obtaining a node). The large scale structure of the universe resembles a honeycomb with voids, surrounded by sheets, that meet at filaments, that meet at spheroidal nodes, that are punctuated by galaxies. Baryons collapse in nodes, filaments [11], and perhaps even in sheets (see Section 3), fragmenting into multiple galaxies and stars with a wide distribution of masses.

At the time t_{eq} of equal radiation and matter densities, the warm dark matter cut-off function has the approximate form $\tau^2(k)=\exp\left(-k^2/k_{fs}^2\left(t_{eq}\right)\right)$ with $k_{fs}\left(t_{eq}\right)$ given in [4]. After t_{eq} the Jeans masses M_{Jh} and M_{Jb} decreas as $a^{-3/2}$, and non-linear regeneration of small scale structure occurs as soon as relative density fluctuations approach unity. Warm dark matter only simulations obtain the cut-off factor $\tau^2(k)$ corresponding to non-linear regeneration of small scale structure, see [12]. With the non-linear $\tau^2(k)$ from [12], we obtain **Figure 7**. For $k_{fs}\left(t_{eq}\right)\approx 1\ \text{Mpc}^{-1}$, 2 Mpc^{-1}, or 4 Mpc^{-1} "first galaxies" and stars form approximately at the red, blue, or green dot, at $z\approx 8.0$, 8.6, or 9.3, and $M_b\approx 1\times 10^9 M_\odot$, $3\times 10^8 M_\odot$, or $3\times 10^7 M_\odot$, respectively. Baryons collapse before warm dark matter, so including baryons in the simulations should obtain a larger non-linear regeneration effect.

Figure 8 is the same as **Figure 7**, but for 3 standard deviation fluctuations instead of 4. For $k_{fs}\left(t_{eq}\right)\approx 1\ \text{Mpc}^{-1}$, 2 Mpc^{-1}, or 4 Mpc^{-1}, 3σ fluctuations form galaxies approximately at the red, blue, or green dot, at $z\approx 6.0$, 6.6, or 7.1, and $M_b\approx 1\times 10^9 M_\odot$, $2\times 10^8 M_\odot$, or $2\times 10^7 M_\odot$, respectively.

We conclude that the warmest dark matter consistent with reionization has $v_{hrms}\approx 395$ m/s, and $k_{fs}\left(t_{eq}\right)\approx 2\ \text{Mpc}^{-1}$. This tentative result needs a correction from 3D simulations that include the formation of galaxies in filaments, and possibly in sheets, and both warm dark matter (free-streaming and velocity

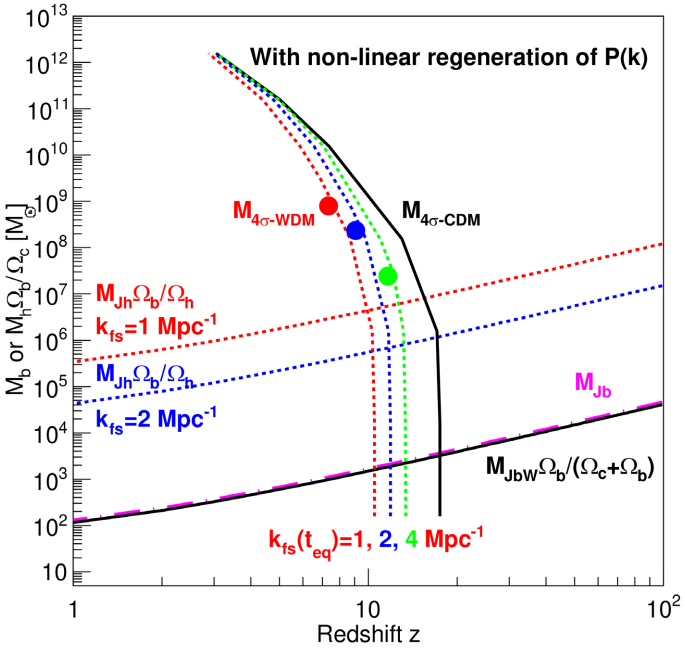

Figure 7. The following linear masses are presented as a function of redshift z: the baryon only Jeans mass M_{Jb}, the warm dark matter only Jeans masses M_{Jh} (times Ω_b/Ω_c) for the ΛWDM$_1$ and ΛWDM$_2$ scenarios, and the baryon mass for cold dark matter halos with a full complement of baryons $M_{JbW}\Omega_b/(\Omega_c+\Omega_b)$, see text. Also presented are the masses for the ΛCDM scenario, and for the ΛWDM scenarios with non-linear regeneration of small scale structure from [12], for which 4σ spherically symmetric fluctuations collapse. These lines are only valid above the dots, see text.

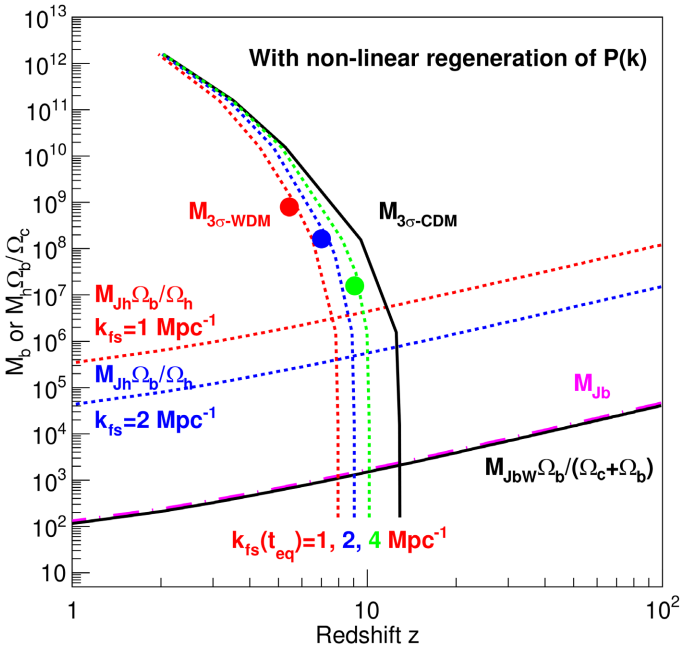

Figure 8. The following linear masses are presented as a function of redshift z: the baryon only Jeans mass M_{Jb}, the warm dark matter only Jeans masses M_{Jh} (times Ω_b/Ω_c) for the ΛWDM$_1$ and ΛWDM$_2$ scenarios, and the baryon mass for cold dark matter halos with a full complement of baryons $M_{JbW}\Omega_b/(\Omega_c+\Omega_b)$, see text. Also presented are the masses for the ΛCDM scenario, and for the ΛWDM scenarios with non-linear regeneration of small scale structure from [12], for which 3σ spherically symmetric fluctuations collapse. These lines are only valid above the dots, see text.

dispersion) and baryons.

5. Baryon Radiation

The conditions for the formation of a star are that the density becomes dominated by baryons, and that these baryons radiate effectively. In this case, as the baryons (hydrogen and helium) radiate, their potential energy drops, and their kinetic energy, *i.e.* their temperature, increases due to gravity. This increase in temperature increases the radiation rate, and the process is run-away, until halted by baryon angular momentum conservation, or by thermonuclear reactions in the core that burn hydrogen into helium at $\approx 1.5 \times 10^7$ K (the *p*-*p* chain reaction) and a star is born on the main sequence. An example is presented in Figure 9.

For warm dark matter, baryons do dominate the core (if angular momentum is sufficiently small), see Figure 2. For cold dark matter, baryons do not initially dominate the core, see Figure 1, so a first stage of radiation results in cooling until baryons dominate the core. For the formation of first stars in the ΛCDM scenario I refer the reader to text books [13] [14] [15]. In the following, we focus our attention on warm dark matter.

Let us consider baryon energy loss by radiation. Channels considered for first generation ("Population III") stars are the molecular hydrogen H_2 channels (the H^- channel, and the H_2^+ channel), and the atomic hydrogen channels, *i.e.* Lyman-*α* transitions [16] [17]. The atomic hydrogen channels open up and dominate at $T_b \gtrsim 10^4$ K, while H_2 channels dominate at lower temperatures. The

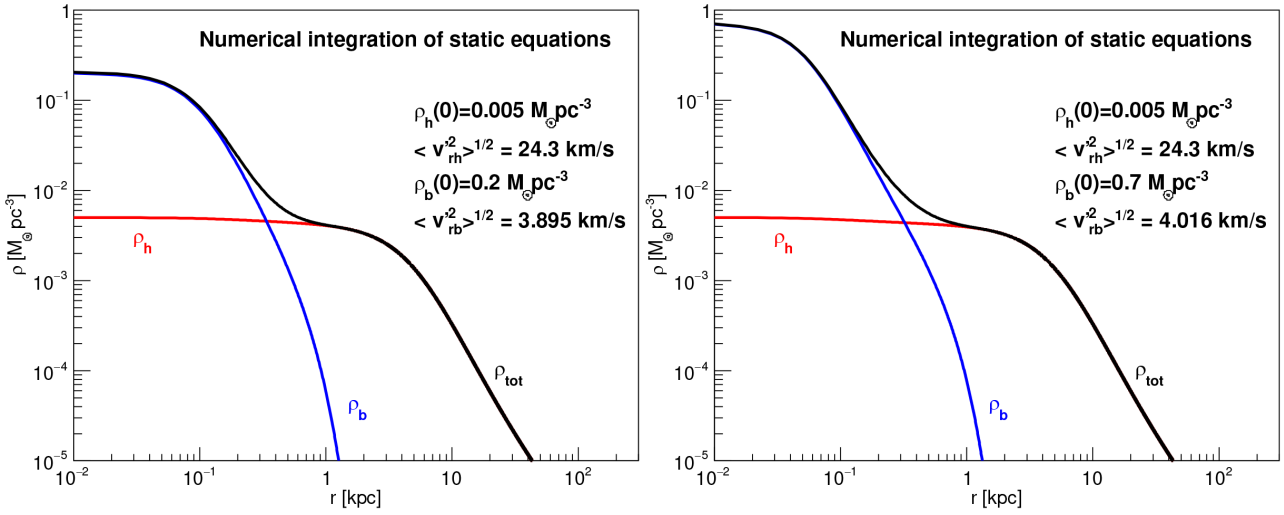

Figure 9. These two solutions to the static equations illustrate the effect of energy loss due to baryon radiation. The core baryon density $\rho_b(0)$ has been increased from $0.2 M_\odot/\text{pc}^3$ in the left panel, to $0.7 M_\odot/\text{pc}^3$ in the right panel. The baryon velocity dispersion was increased from $\langle v_{rb}^2 \rangle^{1/2} = 3.895$ km/s (corresponding to $v_{b\text{rms}}(1) = 21.2$ m/s) to 4.016 km/s to conserve the baryon mass (out to $r = 300$ kpc) $M_b = 4.7 \times 10^6 M_\odot$. The energy (potential plus kinetic of baryons and dark matter out to $r = 300$ kpc) decreases by 1.5×10^{47} J, corresponding to 160 eV per H atom. The baryon temperature increases from $T_b = 1838$ K to 1954 K. The transition from the left to the right panel occurs in $\approx 10^{13}$ s, when the universe is $\approx 2 \times 10^{16}$ s old at $z = 9$.

dominant channel of interest at low temperature is the H^- channel:

$$H + e^- \rightarrow H^- + \gamma$$

$$H^- + H \rightarrow H_2 + e^-. \quad (21)$$

As an example, consider Figure 2. The resolution of our simulation allows us to follow the core down to $r_{\min} = 0.7$ kpc. At this radius the baryon density raises to $0.024 M_\odot / \text{pc}^3$, corresponding to a number density $n = 1\,\text{cm}^{-3}$, $T_b = 447$ K, and an energy 0.058 eV per hydrogen atom. The corresponding cooling function is $\approx 3 \times 10^{-26}$ erg cm^3·s^{-1} [16], and the inverse of the cooling rate is 3×10^{12} s. The age of the universe at the formation of this halo, is 7×10^{15} s. So even the H_2 cooling channel is effective. This calculation is conservative since a rough estimate of the baryon core temperature, using (8), and (11) at the pivot point, exceeds the atomic hydrogen channel threshold $T_b \approx 10^4$ K, even without including heating due to shocks at $r \approx 0$.

As another example, consider the baryon density peak in the sheet of Figure 4. This peak has a density $\rho_b = 0.0023 M_\odot / \text{pc}^3$, corresponding to $n = 0.1\,\text{cm}^{-3}$, $T_b = 94$ K, and a hydrogen atom kinetic energy 0.012 eV (these values are limited by the resolution of the simulation). The cooling function is $\approx 7 \times 10^{-29}$ erg cm^3·s^{-1} [16]. The corresponding inverse of the cooling rate is 3×10^{14} s. The age of the universe at the formation of this sheet, is 3×10^{15} s. So, even for a sheet with hydrogen at this low temperature, the H_2 cooling channel may be marginally effective (a full detailed simulation is needed for confirmation). We have not included the shock observed in Figure 4: its velocity corresponds to $\Delta T_b = 2.7 \times 10^4$ K.

A realistic, high resolution, and detailed simulation concludes that stars do indeed form in filaments [11].

6. Estimate of Dark Matter Properties

The redshift at half reionization from the Planck mission is 7.7 ± 0.7 [5]. From the rest-frame ultra-violet luminosity distribution of galaxies, most of the reionization occurs in the redshift range 8 to 5.7, with a possible slow start at about $z \approx 10$, and with half-reionization at approximately 7.3 [18]. Star formation begins at about $z \approx 10$ [18] [19]. So the onset of reionization lies in the approximate redshift interval from 10.0 to 8.2. This implies that $200\,\text{m/s} \lesssim v_{h\text{rms}}(1) \lesssim 395\,\text{m/s}$, corresponding to $4\,\text{Mpc}^{-1} \gtrsim k_{\text{fs}}(t_{\text{eq}}) \gtrsim 2\,\text{Mpc}^{-1}$, see the green and blue dots in Figure 7 and Figure 8. These estimates include the non-linear regeneration of small scale structure obtained from dark matter only simulations [12], *i.e.* excluding the contribution from baryons that should be significant, and does not include galaxy formation in filaments and sheets.

7. Conclusions

By numerical integration of hydro-dynamical equations, we are able to obtain the density runs $\rho_h(r)$ and $\rho_b(r)$ of relaxed elliptical and spiral galaxies

starting from primordial linear density-velocity-gravitational perturbations. The dark matter halo acquires a core due to the warm dark matter velocity dispersion. Baryons dominate the core density if angular momentum is below a threshold. These baryons radiate, and collapse, and their temperature increases, due to gravitation. The collapse is run-away until stopped by baryon angular momentum conservation, or by thermonuclear reactions that give birth to stars.

From **Figures 6-8** we conclude that the onset of reionization in the ΛWDM scenarios is delayed with respect to ΛCDM. For spherically symmetric perturbations, and neglecting non-linear regeneration of small scale structure, we find that the warmest dark matter consistent with reionization has $k_{\text{fs}}\left(t_{\text{eq}}\right) \approx 3\ \text{Mpc}^{-1}$, corresponding to $v_{h\text{rms}}(1) \approx 270\ \text{m/s}$, with first galaxies with masses M_b of order $10^8 M_\odot$ (that may fragment), see **Figure 6**. However, taking into account the non-linear regeneration of small scale structure (obtained from warm dark matter only simulations [12]), we find that the warmest dark matter consistent with reionization has approximately $k_{\text{fs}}\left(t_{\text{eq}}\right) \approx 2\ \text{Mpc}^{-1}$, corresponding to $v_{h\text{rms}}(1) \approx 395\ \text{m/s}$, see **Figure 7** and **Figure 8**.

From the measured redshift at half-reionization, and the rest frame ultra-violet luminosity distributions of galaxies, that determine the history of the star formation rate, we estimate $200\ \text{m/s} \lesssim v_{h\text{rms}}(1) \lesssim 395\ \text{m/s}$, and $4\ \text{Mpc}^{-1} \gtrsim k_{\text{fs}}\left(t_{\text{eq}}\right) \gtrsim 2\ \text{Mpc}^{-1}$. The corresponding thermal relic mass m_h depends on the temperature at which dark matter decouples from the standard model sector, and on the spin of dark matter particles, see Table 1 of [8].

This preliminary study needs to be extended to non-spherically symmetric perturbations, with high resolution 3D simulations that include dark matter (both free-streaming and velocity dispersion) and baryons, including the baryon physics that obtains the observable stellar luminosities, e.g. an extension of the studies in [11].

We have made *three independent* measurements of the warm dark matter adiabatic invariant $v_{h\text{rms}}(1)$, and hence of the dark matter temperature-to-mass ratio $T_h(a)/m_h$: 1) From approximately 60 spiral galaxy rotation curves [1] [2]; 2) From galaxy stellar mass distributions at $z = 3, 4.5, 6, 7$, and 8 [6]; and 3) The present measurement from reionization. Each of these measurements has its issues. However, taken together, their consistency (within uncertainties that are still large, and a mild tension with the present measurement), and their agreement with the no freeze-in and no freeze-out warm dark matter scenario [8], is quite remarkable. Discrepancies with several limits that can be found in the literature are discussed in [8]. See also section 4, and [20].

Conflicts of Interest

The author declares no conflicts of interest regarding the publication of this paper.

References

[1] Hoeneisen, B. (2019) *International Journal of Astronomy and Astrophysics*, **9**,

71-96. https://doi.org/10.4236/ijaa.2019.92007

[2] Hoeneisen, B. (2019) *International Journal of Astronomy and Astrophysics*, **9**, 355-367.

[3] Hoeneisen, B. (2021) *International Journal of Astronomy and Astrophysics*, **11**, 489-508. https://doi.org/10.4236/ijaa.2021.114026

[4] Boyanovsky, D., de Vega, H.J. and Sanchez, N.G. (2008) *Physical Review D*, **78**, Article ID: 063546. https://doi.org/10.1103/PhysRevD.78.063546

[5] Zyla, P.A., *et al.* (Particle Data Group) (2020) *Progress of Theoretical and Experimental Physics*, **2020**, 083C01.

[6] Hoeneisen, B. (2020) *International Journal of Astronomy and Astrophysics*, **10**, 203-223. https://doi.org/10.4236/ijaa.2020.103011

[7] Weinberg, S. (2008) Cosmology. Oxford University Press, Oxford.

[8] Hoeneisen, B. (2022) *International Journal of Astronomy and Astrophysics*, **12**, 94-109. https://doi.org/10.4236/ijaa.2022.121006

[9] Binney, J. and Tremaine, S. (2008) Galactic Dynamics. 2nd Edition, Princeton University Press, Princeton. https://doi.org/10.1515/9781400828722

[10] Press, W.H. and Schechter, P. (1974) *The Astrophysical Journal*, **187**, 425-438. https://doi.org/10.1086/152650

[11] Gao, L. and Theuns, T. (2007) Lighting the Universe with Filaments. https://arxiv.org/pdf/0709.2165.pdf https://doi.org/10.1126/science.1146676

[12] Markovič and Viel, M. (2013) Lyman-α Forest and Cosmic Weak Lensing in a Warm Dark Matter Universe. Cambridge University Press, Cambridge. https://doi.org/10.1017/pasa.2013.43

[13] Stiavelli, M. (2009) From First Light to Reionization: The End of the Dark Ages. Wiley-VCH, Weinheim. https://doi.org/10.1002/9783527627363

[14] Loeb, A. (2010) How Did the First Stars and Galaxies Form? Princeton Univ. Press, Princeton. https://doi.org/10.1515/9781400834068

[15] Mo, H., van den Bosch, F. and White, S.D.M. (2010) Galaxy Formation and Evolution. Cambridge Univ. Press, Cambridge. https://doi.org/10.1017/CBO9780511807244

[16] Glover, S. (2004) The Formation of the First Stars in the Universe. https://arxiv.org/pdf/astro-ph/0409737.pdf

[17] Maio, U. and Matteo, V. (2021) The First Billion Years of a Warm Dark Matter Universe. https://arxiv.org/pdf/1409.6718.pdf

[18] Robertson, B.E., Ellis, R.S., Furlanetto, S.R. and Dunlop, J.S. (2015) *ApJ*, **802**, L19. https://doi.org/10.1088/2041-8205/802/2/L19

[19] Bouwens, R.J., Illingworth, G.D. and Oesch, P.A. (2015) *ApJ*, **803**, 34. https://doi.org/10.1088/0004-637X/803/1/34

[20] Paduroiu, S. (2022) *Universe*, **8**, 76. https://doi.org/10.3390/universe8020076